Available online at www.sciencedirect.com
ScienceDirect
Journal of Nuclear Materials 367–370 (2007) 298–304
journal of nuclear materials
www.elsevier.com/locate/jnucmat

Study of cascades damage in Ni by MD with different interatomic potentials

Z. Yao [a,*], M.J. Caturla [b], R. Schäublin [a]

[a] Ecole Polytechnique Fédérale de Lausanne (EPFL), Centre de Recherches en Physique des Plasmas, Association Euratom – Confédération Suisse, 5232 Villigen PSI, Switzerland
[b] Departament de Fisica Aplicada, Facultat de Ciencies. Fase II Universitat d'Alacant, E-03690 Alacant, Spain

Abstract

Molecular dynamics (MD) simulations, performed with embedded atom potentials, are used to understand the formation of defects following displacement cascades in Ni. Different empirical potentials, presenting large differences in stacking fault energy (SFE), are used. Simulations were conducted with primary knock-on (PKA) atom energies of 5–40 keV at a temperature of 10 K. Defects include, depending on the potential, individual point defects (vacancies and interstitials), dislocation loops and stacking fault tetrahedra (SFT). The results are related to TEM observations, and the mismatch between these two pictures is discussed. It appears that in a collision cascade, the formation of an SFT does not depend only on the SFE but also on other parameters such as the mobility of vacancies and self-interstitials, or the presence of replacement collision sequences. Based on these calculations we suggest that the formation of clusters of vacancies is a prerequisite to the formation of SFTs.

1. Introduction

Irradiation-induced defects in pure Ni have been extensively studied in the past [1–6]. These experiments showed that defects in Ni consist of vacancy type defects, such as SFT and voids, and interstitial dislocation loops. A longstanding question in Ni is the occurrence of the SFT, for which, at a given irradiation dose, controversial number densities are given in the literature. In Cu, which has an SFE of about 70 mJ m^{-2} [7], 90% of the damage consists of SFT. When considering the SFE of Ni, 125 mJ m^{-2} [8], it is expected that the formation of SFTs would be difficult. In the literature, the ratio of SFTs to other defects in Ni varies between 28% [2] and 90% [1], and data in [2] indicates a variation of the ratio with the dose. Recently detailed observations [6] indicate that the SFT ratio is 30–50%. This can be explained by the fact the average SFT size, at 1.5 nm, is at the limit of the weak beam TEM technique, which renders their observation difficult and are usually classified as unidentified defects.

MD simulations are helpful to understand the role of various properties of the material in the formation of irradiation-induced defects. They have

* Corresponding author. Present address: Department of Materials, University of Oxford, Parks Road, Oxford OX1 3PH, UK. Fax: +44 1865 273767.
E-mail address: zhongwen.yao@materials.oxford.ac.uk (Z. Yao).

0022-3115/$ - see front matter © 2007 Elsevier B.V. All rights reserved.
doi:10.1016/j.jnucmat.2007.03.136

been widely used for more than two decades to model displacement cascades generated by a primary knocked-on atom (PKA). King et al. [9] performed cascades of 500 eV and Diaz de la Rubia et al. [10] performed 5 keV cascades in Ni and Cu using the embedded atom method [11]. These studies showed that more clustering occurs in Cu than in Ni. Almazouzi et al. [12] reported the long term evolution of the defects produced by displacement cascades in Ni, using the interatomic potential developed by Cleri and Rosato [13] and later modified in order to properly describe high energy scattering. They performed displacement cascade simulations for PKA energies ranging from 0.5 keV to 30 keV, with constant volume, periodic boundary conditions and a temperature of 100 K. Interestingly, the potential used in these later studies predicts an SFE of 300 mJ m^{-2}, which is more than twice the experimental value [8]. While extremely valuable results were obtained using these potentials, the role of the SFE in the formation of the defect structure following a displacement cascade can be questioned and has never been studied by simulation.

In the present work, various potentials for Ni, presenting large differences in the SFE, are used in the simulation of displacement cascades. The resulting damage is analyzed using the Wigner Seitz cell and the common neighbor analysis method and the defects are compared to experimental observations. The implications of the observed differences on the various parameters of the material described by the empirical potentials are discussed.

2. Simulation method

In the present work, four different empirical potentials were employed for the MD simulations in order to investigate the effect of the SFE on cascade evolution. MD simulations were conducted using the mdcask code [14]. Table 1 summarizes the characteristics of these potentials and compares them to experimental values. The reported values are the lattice parameter (a_0), the range of the potential (r_{cut}), the displacement threshold energy (E_d), the elastic constants C_{11}, C_{12} and C_{44}, the bulk modulus (B) and the SFE (γ). The displacement threshold energy was deduced from simulations by starting the PKA in random crystallographic directions with increasing energies until the atom was displaced from its lattice site and would not return to it after cooling. The range of values for the displacement threshold energy in Table 1 corresponds to the minimum and maximum values obtained in the simulations, which relate respectively to the soft ($\langle 1\,0\,0\rangle$) and the hard ($\langle 1\,1\,0\rangle$) crystallographic directions.

The so-called Farkas-I and Farkas-II potentials [15] were tailored to specific SFE values, corresponding to half and to exactly the experimental value from reference [8], respectively. While the so-called Cleri–Rosato is an earlier potential [13] frequently used, the SFE is more than twice the experimental value. The A.A is a modified Cleri–Rosato potential, to better account for the high energy collisions [16]. This is done by using the universal potential of Ziegler et al. [17] instead of the Cleri–Rosato potential, for interatomic distances smaller than 1 Å. The smooth connection between the two potentials was fitted by a spline. The resulting displacement threshold energy is then closer to the experimental value than the one given by the original potential. The elastic properties and the SFE remain the same, as they are related to interatomic distances beyond the range of the part modified by the universal potential.

3. SFT formation

In order to evaluate the potentials, they were applied to the formation of a well-defined single SFT. Silcox and Hirsch [18] proposed the following SFT formation mechanism. A vacancy disc nucleates on a $\{1\,1\,1\}$ plane, changes its shape to a triangular

Table 1
Bulk properties of Ni as measured experimentally and simulated with the various empirical potentials deployed in this work: lattice parameter a_0, elastic constants C_{11}, C_{12} and C_{44} bulk modulus B and stacking fault energy γ

	a_0/r_{cut} (Å)	Threshold energy (eV)	C_{11}	C_{12}	C_{44}	B (10^{11} Pa)	γ (mJ m^{-2})
Experimental [8]	3.523	40	2.47	1.47	1.25	1.81	125
Farkas-I [15]	3.519/4.7895	30–60	–	–	–	–	61
Farkas-II [16]	3.523/5.8038	15–25	2.47	1.48	1.25	1.81	125
Cleri–Rosato [13]	3.523/5.8714	90–300	2.33	1.54	1.28	1.80	300
A.A [16]	3.523/4.6485	40–80	2.33	1.54	1.28	1.80	300

r_{cut} is the potential range.

one with ⟨1 1 0⟩ edges and subsequently collapses into an SFT. An SFT can be obtained in MD simulation by using the same mechanism [19,20]. Wirth et al. using MD simulations showed in detail that indeed the Silcox and Hirsch mechanism occurs at atomic scale level and results in the collapse of this platelet into an SFT [21]. A triangular platelet of vacancies is placed onto a {1 1 1} plane by removing atoms from it (Fig. 1(a)). Then the sample containing the vacancy platelet of a given size is annealed at a given temperature and time until it collapses to an SFT, provided the potential and conditions (size, temperature and anneal time) allow it.

According to experimental work [3–6], the observed SFT mean size in irradiated Ni remains approximately 1.5 nm for irradiations at room temperature, over a wide range of irradiation doses, and grows to 3.5 nm for an irradiation temperature of 250 °C. Consequently, the size of simulated SFTs was selected to range from ~0.7 to ~3 nm. According to the above mentioned mechanism decomposed in three steps, a triangular vacancy platelet was first formed (Fig. 1(a)). The size of the resulting SFT is pre-defined by the size of this triangle. A triangle of 6, 15 and 66 vacancies corresponds to an SFT that is 0.7, 1.5 and 3 nm in size, respectively.

A simulation box of $24 \times 24 \times 24$ in lattice units was used for the relaxation at temperatures from 500 K to 800 K. The duration of annealing ranged from 1 to 2 ps. After annealing, the system potential energy was minimized by using the conjugate gradient method in order to find the relaxed positions of the atoms.

In order to identify the defect configuration, the common neighbor analysis (CNA) method was used. It allows identifying the coordination number of the atoms, which relates to either an hexagonal compact (hcp), face centered cubic (fcc) or body centered cubic (bcc) structure, or none of these. The main results are summarized as follows. The platelet of 6 vacancies did not collapse into an SFT, regardless of the annealing conditions, but it formed a void (Fig. 1(b)) at relaxations above 800 K, for all selected potentials. Below this temperature it remained in a platelet shape without any transformation. The platelet of 15 vacancies collapsed into an SFT (Fig. 1(c)) when using Farkas-I and Farkas-II potentials, at 500 K. It remained in the original platelet shape when Cleri–Rosato and the modified Cleri–Rosato potentials were used. The different SFE (see Table 1) explains this phenomenon. Lower SFE implies that Shockley partial emission is favored and forms the stacking faults on the conjugate {1 1 1} planes, resulting in the SFT. The platelet of 66 vacancies easily collapsed to an SFT at 500 K, for all four potentials. The collapse occurred even with the Cleri–Rosato potential presenting the highest SFE of all.

4. Cascade simulation

A number of cascade calculations have been carried out using different conditions. Before launching the PKA, the simulation box was annealed by velocity rescaling of all atoms for 2 ps in order to reach the desired temperature. Longer anneal times did

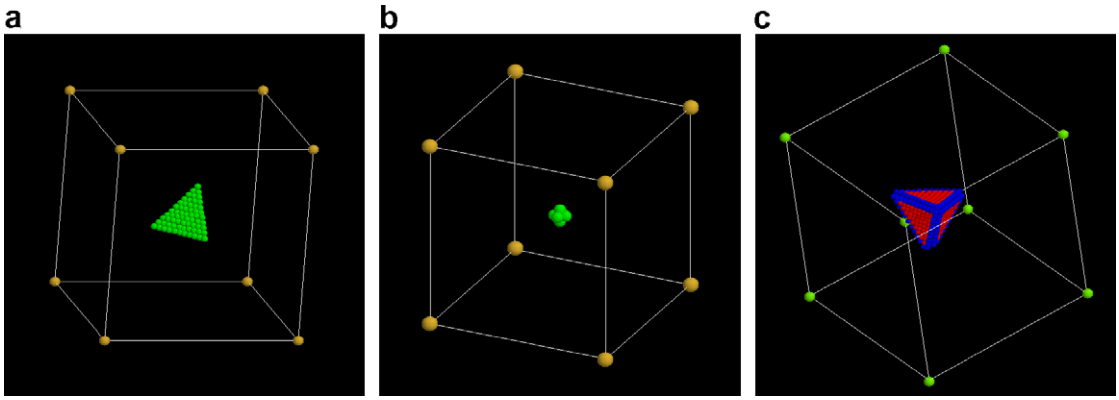

Fig. 1. Evolution of a triangular platelet of vacancies in Ni after anneal at 800 K for 2 ps and relaxation, depending on the number of vacancies: (a) original triangular platelet of 66 vacancies, (b) a void formed by relaxing a 6-vacancy platelet and (c) a fully developed SFT collapsed from a 15-vacancy platelet, all using Cleri–Rosato potential. The green balls represent vacancies, red balls are hcp-coordinated atoms and blue balls are atoms with non-fcc, non-hcp and non-bcc coordination. (For interpretation of the references to colour this figure legend, the reader is referred to the web version of this article.)

not affect the resulting damage structure. One atom from the system was then selected as the PKA, with an appropriate shooting angle, position and energy. In order to avoid channeling, the angle should not be too close to a crystallographic direction. Temperature control after the PKA is achieved by a thermal bath consisting of a few atomic layers at the boundaries of the sample whose temperature is controlled by velocity rescaling every 100 steps (100 fs) to mimic thermal conduction to the bulk. Fig. 2(a)–(c) shows typical cross sectional views of a Ni specimen in which a 40 keV cascade evolves. Fig. 2(d) and (e) indicate that temperature and potential energy change with time, and a thermal spike appears within 1.5–2 ps after the PKA. Cascades were repeated three times in order to obtain average values that are statistically meaningful.

Cascades with energy 30 keV are selected to compare the influence of the four potentials on the resulting damage. The results of CNA are shown in Table 2 and Fig. 3 and can be summarized as follows. Farkas-I and Farkas-II potentials give rise to similar defect structures. No large clusters are formed and defects are scattered in the form of small clusters or individual point defects, which might be caused by a reduced mobility of vacancies and interstitials during the collision cascade. Farkas-II gives a higher density of defects than Farkas-I. Farkas-I gives rise to small loops. Surprisingly, there are no visible SFT or SFT-like structures, even though the SFE is low. However, Farkas-I, with the lowest SFE, does produce more hcp atoms, which are found in the stacking fault of the fcc structure. Here calculation of defect

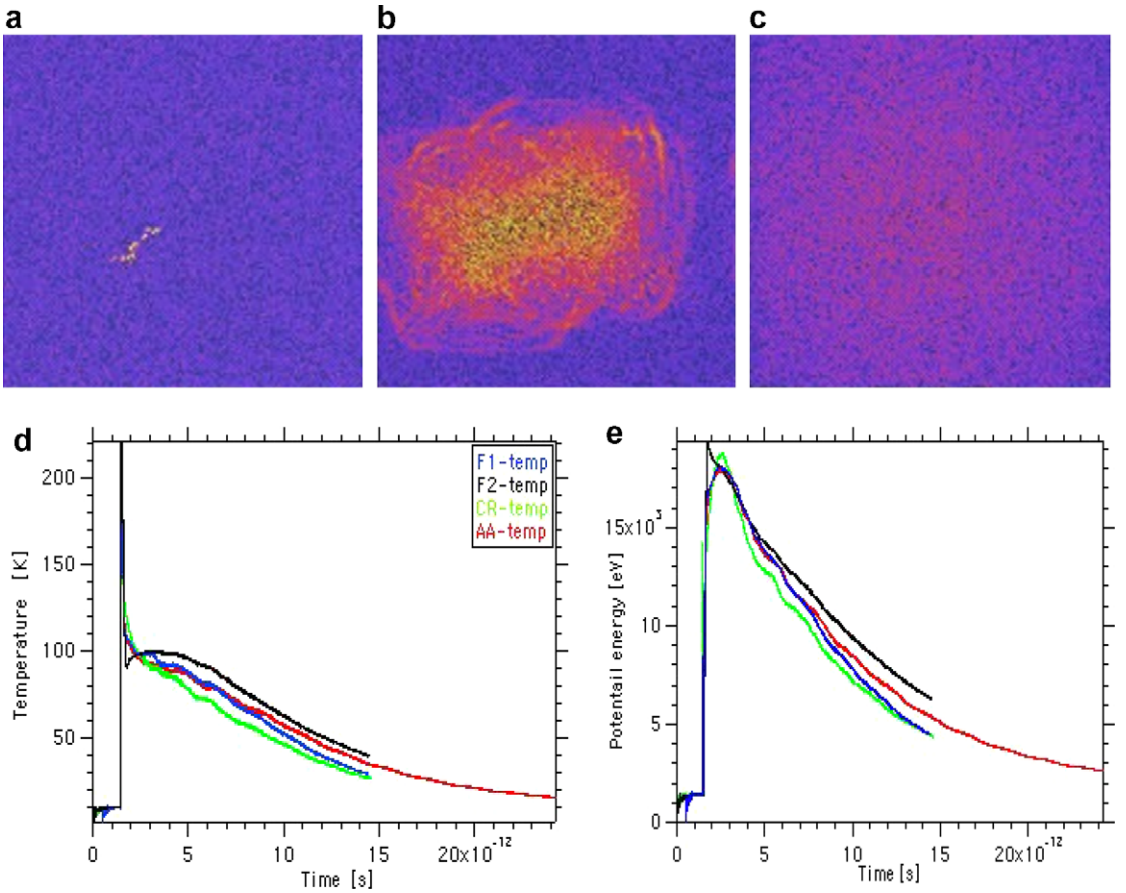

Fig. 2. View in cross section of the evolution of 40 keV cascade in Ni simulated by MD at (a) 0.1 ps showing first collisions, at (b) 0.8 ps showing shock wave propagation and hot core and at (c) 25 ps showing the cool down and the recrystallization of the molten core, respectively, after the PKA. The sample is 1 million atoms and the side length is 22.9 nm. Color represents the kinetic energy (blue: cold, yellow: hot). (d) Temperature and (e) potential energy as a function of time and of the potentials used. Farkas-I: F1, Farkas-II: F2, Cleri–Rosato: CR, modified Cleri–Rosato: AA. (For interpretation of the references to colour this figure legend, the reader is referred to the web version of this article.)

Table 2
Average damage resulting from 30 keV cascade as a function of the potential

	Number of interstitials	Number of vacancies	Number of clusters (i/v)	hcp atoms/non-hcp, -fcc atoms
FI	66	66	13/7	97/1363
FII	141	141	15/21	12/3522
Cleri–Rosato	169	169	30/31	931/1723
Cleri–Rosato-A.A	129	129	25/20	174/1902

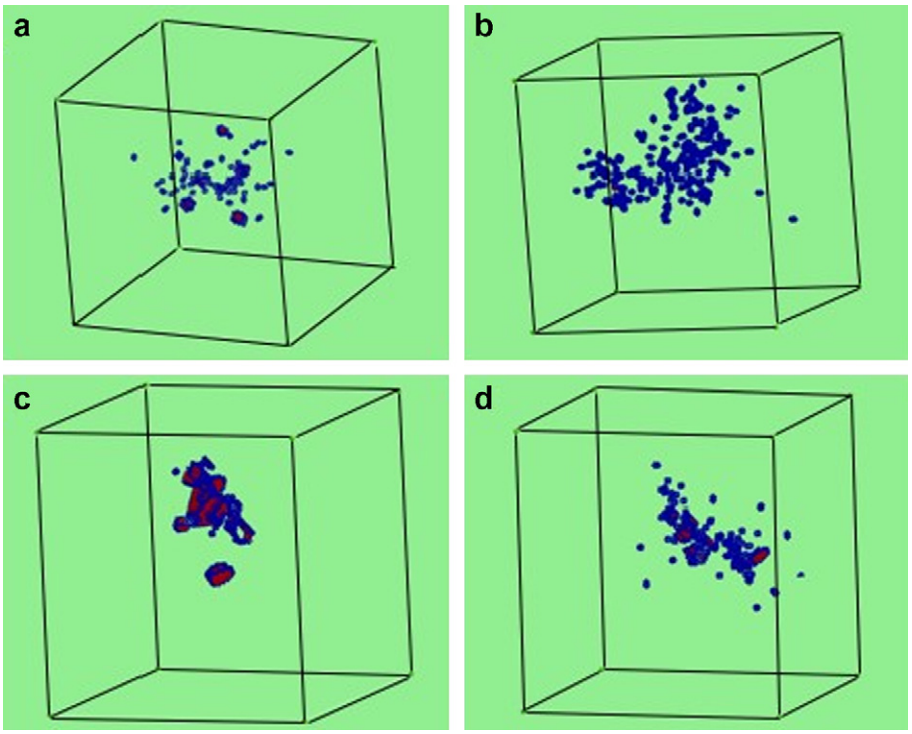

Fig. 3. (a–d) The resulting damage produced by a 30 keV cascade using Farkas-I, Farkas-II, Cleri–Rosato and modified Cleri–Rosato potential, respectively. Red balls show hcp-coordinated atoms (stacking fault related) and blue balls are atoms that are non-hcp, non-fcc,and non-bcc coordinated. (For interpretation of the references to colour this figure legend, the reader is referred to the web version of this article.)

migration energy is suggested to be applied in the future for understanding the role of defect mobility in the clustering during cooling.

In Fig. 3(c) and (d), produced with the Cleri–Rosato potential with and without the fit to the ZBL potential respectively, SFT-like structures appear close to the cascade core. Also, an isolated interstitial loop can be seen in Fig. 3(c). The maximum number of Frenkel pairs is obtained with the Cleri–Rosato potential without the high energy part, which in fact has the largest displacement threshold energy (90–200 eV). Since hcp atoms reflect the stacking fault areas, it appears that the Cleri–Rosato potential (Fig. 3(c)) shows the largest number of stacking faults, even though the potential presents the highest SFE (300 mJ m^{-2}).

The number of defects or Frenkel pairs produced by each potential for PKA energies from 5 keV to 40 keV, is reported in Table 3, together with the number of Frenkel pairs evaluated using the NRT model [22], shown in parenthesis. The NRT value is different for different potentials because this model depends on the displacement threshold energy. The number of Frenkel pairs produced by simulation for a given PKA energy varies similarly. According to literature [23], the number of Frenkel

Table 3
Average number of resulting Frenkel pairs (NFP) produced by MD cascade with different PKA energy and potentials at 10 K

	Farkas I	Farkas II	Cleri–Rosato	Modified Cleri–Rosato
5 keV	NA	47 (100)	– (20)	9 (50)
10 keV	17 (100)	76 (200)	369 (40)	49 (100)
20 keV	37 (200)	107 (400)	74 (80)	104 (200)
30 keV	66 (300)	141 (600)	169 (120)	129 (300)
40 keV	– (400)	266 (800)	1335 (160)	272 (400)

The NRT values are reported in parenthesis.

pairs produced in MD simulations is about 30% of the NRT number, when the PKA energy is larger than 5 keV. In this study all potentials but one produce a similar behavior.

In the case of Cleri–Rosato potential however, PKAs with energies from 5 keV to 40 keV produce a large number of Frenkel pairs, higher than the NRT value. Therefore, the Cleri–Rosato potential should in principle be excluded as an adequate choice. However, it should be noted that in Fig. 3(c) an SFT-like structure and an interstitial loop are observed, which is the closest to the irradiation-induced microstructure observed in the TEM.

5. Conclusions

MD simulations have been performed to understand the formation of defects following displacement cascades in Ni, and its dependence on the empirical potential used. The results of SFT collapse tests show that a platelet of 6 vacancies did not collapse to an SFT regardless of the annealing conditions, but formed a void above 800 K for all selected potentials. The platelet of 15 vacancies collapsed into an SFT when simulated with Farkas-I and Farkas-II potentials, while the platelet of 66 vacancies easily collapsed to an SFT at 500 K for all applied potentials, even for the one with a high SFE, 300 mJ m^{-2}. For a size of 15 vacancies our results indicate that it is the SFE that drives the formation of the SFT. The lower the SFE, the easier the formation of the SFT.

In the case of damage produced by a displacement cascades, the situation is less clear. It appears that the largest number of stacking faults and the closest features to an SFT are obtained with the potential of Cleri–Rosato, which is characterized by the highest SFE (300 mJ m^{-2}) and the highest displacement threshold energies. However, the modified Cleri–Rosato, with the same SFE but a reasonable displacement threshold energy, does not produce such SFT-like features. Moreover, when using Farkas I or Farkas-II, the potential yielding the SFE closest to the experimental value, no stacking faults or large clusters are observed. The lack of clustering of defects observed in these potentials could be the reason for the lack of SFT formation, despite the low SFE, which might be relate to the reduced mobility of defects with these interatomic potentials.

Acknowledgments

The Swiss National Science Foundation is acknowledged for financial support. The Paul Scherrer Institute is acknowledged for the overall use of the facilities. One of the authors (MJC) thanks the Barcelona Supercomputer Center for the use of MareNostrum and the Spanish MEC for support under the Ramón y Cajal program.

References

[1] M. Kiritani, N. Yoshida, S. Ishino, J. Nucl. Mater 122&123 (1984) 602.
[2] S.J. Zinkle, L.L. Snead, J. Nucl. Mater 225 (1995) 132.
[3] Z. Yao, R. Schäublin, M. Victoria, J. Nucl. Mater 329–333 (2002) 1127.
[4] Z. Yao, R. Schäublin, M. Victoria, J. Nucl. Mater 329–333 (2004) 1127.
[5] R. Schäublin, Z. Yao, M. Victoria, Philos. Mag. 85 (2005) 769.
[6] Z. Yao, The relationship between the irradiation induced damage and the mechanical properties of single crystal Ni, PhD thesis #3177, EPFL, 2005.
[7] J.P. Hirth, J. Lothe, Theory of Dislocations, Wiley-Interscience Publication, 1982, p. 332.
[8] C.B. Carter, S.M. Holmes, Philos. Mag. A 35 (5) (1977) 1161.
[9] W.E. King, R. Benedek, Phys. Rev. B 23 (1981) 6335.
[10] T. Diaz de la Rubia, R.S. Averback, H. Horngming, J. Mater. Res. 4 (1989) 579.
[11] M.S. Daw, M.I. Baskes, Phys. Rev. B 29 (1984) 6443.
[12] A. Almazouzi, M.J. Caturla, M. Alurralde, T. Diaz de la Rubia, M. Victoria, Nucl. Instrum. and Meth. B 153 (1999) 105.
[13] F. Cleri, V. Rosato, Phys. Rev. B 48 (1993) 22.
[14] T. Diaz de la Rubia, M.W. Guinan, J. Nucl. Mater. 174 (1990) 151.
[15] Y. Mishin, D. Farkas, M.J. Mehl, D.A. Papaconstantopoulos, Phys. Rev. B 59 (5) (1999) 3393.
[16] M.J. Caturla, A Short Course in Molecular Dynamics Simulations with Empirical Potentials, Dept. Fisica Aplicada, Universidad de Alicante, 2003.
[17] J.F. Ziegler, J.P. Biersak, U. Littmark, Stopping and Range of Ions in Solids, vol. 1, Pergamon, New York, 1985.
[18] J. Silcox, P.B. Hirsch, Philos. Mag. 4 (1959) 72.

[19] Y.N. Osetsky, R.E. Stoller, Y. Matsukawa, J. Nucl. Mater 329–333 (2004) 1228.
[20] B.D. Wirth, M.J. Caturla, T. Diaz de la Rubia, T. Khaishi, H. Zbib, Nucl. Instrum. and Meth. B 180 (2001) 23.
[21] B.D. Wirth, V. Bulatov, T. Diaz de la Rubia, J. Nucl. Mater. 283–287 (2000) 773.
[22] M.J. Norgett, M.T. Robinson, I.M. Torrens, Nucl. Eng. Des. 33 (1974) 50.
[23] D.J. Bacon, A.F. Calder, F. Gao, V.G. Kapinos, S.J. Wooding, Nucl. Instrum. and. Meth. B 102 (1995) 37.